Sound generation by steady flow through glottis-shaped orifices

Zhaoyan Zhang,[a] Luc Mongeau,[b] Steven H. Frankel, Scott Thomson, and Jong Beom Park

Ray W. Herrick Laboratories, Purdue University, 140 South Intramural Drive, West Lafayette, Indiana 47907-1077

(Received 21 January 2004; revised 4 June 2004; accepted 17 June 2004)

Although the signature of human voice is mostly tonal, it also includes a significant broadband component. Quadrupolelike sources due to turbulence in the region downstream of the glottis, and dipolelike sources due to the force applied by the vocal folds onto the surrounding fluid are the two primary broadband sound generating mechanisms. In this study, experiments were conducted to characterize the broadband sound emissions of confined stationary jets through rubber orifices formed to imitate the approximate shape of the human glottis at different stages during one cycle of vocal fold vibrations. The radiated sound pressure spectra downstream of the orifices were measured for varying flow rates, orifice shapes, and gas mixtures. The nondimensional sound pressure spectra were decomposed into the product of three functions: a source function F, a radiation efficiency function M, and an acoustic response function G. The results show that, as for circular jets, the quadrupole source contributions dominated for straight and convergent orifices. For divergent jets, whistling tonal sounds were emitted at low flow rates. At high flow rates for the same geometry, dipole contributions dominated the sound radiated by free jets. However, possible source-load acoustic feedback may have hampered accurate source identification in confined flows. © *2004 Acoustical Society of America.* [DOI: 10.1121/1.1779331]

PACS numbers: 43.70.Aj, 43.28.Ra [MSH] Pages: 1720–1728

I. INTRODUCTION

Voice production involves sound generation by turbulent confined jets through an orifice (the glottis) with a time-varying area. The glottis is a slitlike orifice between the vocal folds, located in the airway and connected to the vocal tract. In voice production, the glottis is excited into self-oscillations by the airflow through it, causing a confined pulsating air jet downstream. The motion of the vocal folds is complex, and involves a continuous evolution of the orifice profile. One cycle of the orifice time history may be idealized using a succession of three representative glottal wall profiles: convergent, straight, and divergent. The acoustic waves generated by the pulsating jet flow, which represent the main voice source, are effectively filtered by the articulators forming the vocal tract downstream, such as the mouth and nasal cavity, before being radiated from the lips.

The radiated sound signature in voice production consists of the sum of a periodic component and a random broadband component. The periodic component due to the pulsating flow forced by glottis oscillations dominates at low frequencies in sonorant sounds. This basic tonal voice production mechanism is generally well understood, and can be modeled using a quasi-steady approximation (Zhang *et al.*, 2002b). The (modulated) broadband component, which is presumably related to the turbulence in the air stream, is much smaller in amplitude for phonation at low frequencies. However, broadband sound is an important component of human voice at high frequencies (above approximate 7000 Hz). Similar jet flows are also involved in the generation of fricative consonants, another important component of speech. A better understanding of the broadband sound generation mechanisms is useful in speech applications such as voice diagnostics and high-quality speech synthesis.

There have been relatively few studies on the production of broadband sound from air flow through the larynx and the vocal tract. Early measurements suggested that the broadband noise spectrum is relatively constant in the mid-audio frequency range (Flanagan, 1965). Experimental work by Meyer–Eppler (1953) has suggested that, for fricative consonants, a critical Reynolds number exists below which there is negligible turbulent sound generation. Meyer–Eppler has reported that the sound pressure related to turbulence in the airflow increases with the square of the Reynolds number. Such a scaling law, however, was postulated without rigorous verification through systematic changes in physical model size or working fluid.

Stevens (1998) has reported that the radiated sound pressure from turbulent flow through constrictions is proportional to the third power of jet velocity and the square root of the constriction area. The recent work of Harper (2000) on breathing sounds was again based on a Reynolds number power law. Such models neglect the possible influence of acoustic loading on sound production. The spectrum of the sound pressure for a source such as turbulent flow past an obstacle located in an open space tends to have a broad peak at a constant Strouhal number (Goldstein, 1976). To account for the influence of the acoustic response of cavities and ducts for sources within confined spaces on power law exponents, inverse filtering methods are needed. Many of these

[a]Also at the Institute for Systems Research, University of Maryland, College Park, MD 20742; Electronic mail: zhaoyan@glue.umd.edu

[b]Currently on leave at Ecole Centrale de Lyon, 36 Avenue Guy de Collongue, 69134 Ecully, France.

methods may not yield accurate results when the sound source region is spatially distributed, random, and spatially partially coherent.

Broadband sound generation by confined stationary jets through circular orifices was recently studied by Zhang *et al.* (2002a). An acoustic similarity law was derived, in which the nondimensional sound pressure spectrum was formulated as a product of a source spectral distribution function, a radiation efficiency function, and an acoustic frequency response function. The three functions were separated using a spectral decomposition method, thus allowing the identification of source type and source spectral characteristics. Sound radiation was found to be similar to that of a quadrupole source in tubes, with negligible dipole contribution.

For sound generation by stationary jet flows through glottis-shaped orifices, dipole sources due to the fluctuating pressure on the orifice walls may play a role in addition to the quadrupole sources due to flow turbulence in the region downstream of the orifice (Zhang *et al.*, 2002b). It is believed that the shape of the glottal orifices has an important impact on the behavior of these two sound production mechanisms. In particular, there may exist interactions between vortical flow structures and the sound field in cases where the orifice walls form a divergent diffuser.

Vortex structures in jet flows through orifices have been well described. Johansen (1929) studied water flow through a sharp-edged circular orifice mounted concentrically in a glass pipe. Flow visualization showed an axisymmetric jet with vortex rings. At low Reynolds number, as the flow began to transition from laminar to turbulence, these vortices were shed at a constant Strouhal number. Vortices were also observed to emerge from a sharp-edged two dimensional slit as well as a sharp-edged circular orifice in a rectangular channel by Beavers *et al.* (1970). Vortex sheets were formed with a constant Strouhal number (0.43 for two-dimensional jets and 0.63 for circular jets) over Reynolds numbers ranging from 500 to 3000. Flow visualization of the jet formation process has been performed by Shadle *et al.* (1987) using a dynamic model of the vocal folds consisting of two rectangular shutters. It was found that when the orifice was slightly off-center, the jet attached to the wall closest to the orifice. When obstructions representing false folds were added downstream, however, the jet plume ''straightened out.'' Recently, flow visualization observations have been made for flow through a rigid static divergent glottis model (Dabiri *et al.*, 2001). The jets were found to be skewed, and oscillated randomly. Vortical structures were also observed. The flow separation points moved along the glottis walls as the transglottal pressure was varied, and the flow was very unstable.

Instability waves and related vortex structures are possible sound sources. Relationships between the existence of forced shear layer instability and radiated sound were identified in the experiments of Moore (1977). McGowan (1988) used an aeroacoustic approach to study the source of sound during phonation. He postulated that, in addition to the unsteady volume velocity monopole source, an oscillating force (i.e., a dipole source) arises from the interaction between vortical structures shed from the glottis and the velocity field itself. In measurement using a dynamic mechanical model of the larynx and the vocal tract, Barney and co-workers (1999) found evidence of a vortex train, which contributed to sound radiation due to the interaction with the vocal tract downstream. Hofmans (1998) experimentally and computationally investigated the starting flow through various mechanical models comprising nozzles and orifices. A very complex behavior of interacting vortices due to the jet instability was observed. Frequencies of pressure perturbations associated with the vortex pairing and merging process were in the audible range. Contributions to speech production were postulated.

The present study is an extension of the work of Zhang *et al.* (2002a). The objective was to investigate the possible effects of the orifice geometry on broadband sound generation. The investigation of the source spectral characteristics for different orifice geometries could also allow the development of advanced models for broadband voiced sound in speech synthesis applications. Whistlelike tone generation for geometries featuring a divergent orifice cross-section was encountered, and is also discussed.

II. THEORETICAL BACKGROUND

A brief description is given in this section of the acoustic similarity law and spectral decomposition method derived by Zhang *et al.* (2002a). The readers are referred to the original paper for a detailed analysis and validation.

Consider sound generation by a finite region of turbulence in a long rigid rectangular tube. Assuming a compact source region, the radiated sound pressure spectral density can be expressed as the product of a source spectral distribution function F, a radiation efficiency function M, and a far-field acoustic response term G. The latter describes the effects of sound propagation phenomena from the source region to the observer. The nondimensional sound pressure spectrum, $E=S_{pp}(x,f)/(\frac{1}{2}\rho U^2)^2 d/U$, is presumed to obey the product law (Zhang *et al.*, 2002a):

$$E=F\left(\mathrm{St},\mathrm{Re},\frac{d}{D}\right)M(\mathrm{He})G\left(\mathrm{He},\frac{x_R}{D},R\right), \tag{1}$$

where S_{pp} is the sound pressure spectral density, D is the tube cross-sectional dimension, d is the orifice hydraulic diameter, x_R is the observer location, ρ is the fluid density, and R is the acoustic boundary condition. The hydraulic diameter was defined for the slit-shaped orifice cross sections as 2 times the orifice width. The dimensionless groupings are defined as $\mathrm{Re}=Ud/\nu$, $\mathrm{St}=fD/U$, $\mathrm{He}=fD/c$, where U is the centerline velocity of the jet, ν is the fluid viscosity, f is frequency, and c is the speed of sound.

The radiation efficiency is defined as the ratio of the radiated sound power and the mechanical power driving the sound generation phenomena. For a multipole source of order n in free space, the radiation efficiency function is of the order of $(kD)^{2n}$ (Howe, 1998), where k is the wave number. The radiation efficiency decreases with ascending multipole order. The presence of the confinement changes both the source characteristics and the sound field. At frequencies below the duct cut-on frequency, in which only plane wave

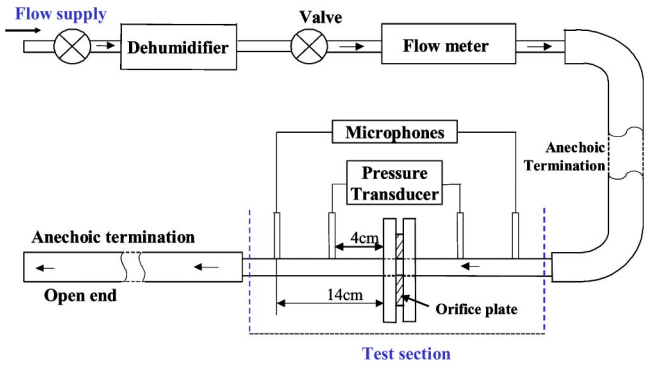

FIG. 1. Schematic of the experimental apparatus.

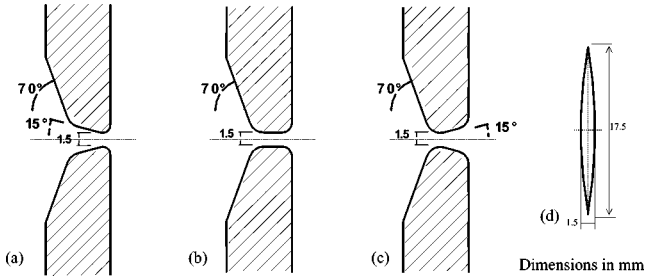

FIG. 2. Cross section of the three orifice passages (a) convergent, (b) straight, and (c) divergent. The flow direction is from left to right. (d) Elevation of the orifice showing the frontal opening area.

propagation is possible and the sound field is essentially one-dimensional, sound radiation is more efficient in tubes than in free space (Howe, 1998). For example, the radiation efficiency of a quadrupole source in tubes is in the form of $(kD)^2$, in contrast with $(kD)^4$ for a quadrupole source in free space $(kD<1)$. As frequency increases above the cut-on frequency, the sound field is three-dimensional and the sound radiation behavior approaches that for free space (Davies *et al.*, 1968). The radiation efficiency accordingly transitions from $(kD)^2$ to $(kD)^4$.

The M and G functions are functions of only the Helmholtz number. Their product forms a new function G_1. For a fixed microphone position, constant acoustic boundary conditions and orifice geometry, Eq. (1) becomes

$$E = F(\mathrm{St},\mathrm{Re})G_1(\mathrm{He}). \tag{2}$$

The three functions can be separated from measured sound pressure spectral data using a spectral decomposition method (Zhang *et al.*, 2002a), assuming a linear source-filter model for the sound generation system. Expressing the nondimensional spectrum using a logarithmic scale, Eq. (2) is rewritten as

$$10\log F(\mathrm{St},\mathrm{Re}) = 10\log E - 10\log G_1(\mathrm{He}). \tag{3}$$

Nondimensional sound spectra may be plotted against the St number and the Re number for values of f and c forming a constant He number. Since the F and G_1 functions are assumed to be independent, surfaces for consecutive He number values should be parallel to each other. They should have the same functional shape and only differ by a constant level difference over the St–Re plane. This level difference is equal to the difference in the value of $10\log G_1$ corresponding to the two He number values considered. By arbitrarily imposing a zero value to the function G_1 at the minimum value of the He number in the experimental data, the G_1 function can then be uniquely constructed over the entire range of He number. This allows $10\log F^k$ functions to be obtained for each combination of the Strouhal number and the Reynolds number using Eq. (3). The final value of the function $10\log F$ is obtained by ensemble-averaging all $10\log F^k$ functions.

It has been shown that the acoustic frequency response function, G, is in good agreement with the transfer function between the radiated acoustic pressure at one fixed location and the strength of an equivalent velocity source located at the orifice, and has a comparatively uniform spectral shape (Zhang *et al.*, 2002a). For a multipole sound source of order n, the G_1 function then follows closely the trend of the M function. Therefore, it is possible to identify the dominant order of the source multipole from the trends in the measured G_1 functions.

III. EXPERIMENTAL APPARATUS

Hardware from a previous study was used (Zhang *et al.*, 2002a). The test section consisted of two rectangular tubes, as illustrated in Fig. 1. Each tube had an inner cross-section 2.25×2.25 cm and was 22.5 cm long. A 6 mm thick rubber glottis-shaped orifice plate with two cover aluminum plates was inserted between the two rectangular tubes. The rubber glottis-shaped orifice plates were built to simulate the human vocal folds geometry, and acted as a constriction to the airflow. Three different orifice geometries (straight, convergent, and divergent) (Fig. 2) were used in the experiments, each representing a typical stage of the phonation cycle. The two tubes were connected to anechoic terminations on both the flow supply and the discharge ends, respectively. The same anechoic terminations were used as in previous studies (Zhang *et al.*, 2002a; Zhang *et al.*, 2002b). The reflection factor of the downstream system was measured using the two-microphone method. Its magnitude is shown in Fig. 3 over the plane wave frequency range. The reflection factor

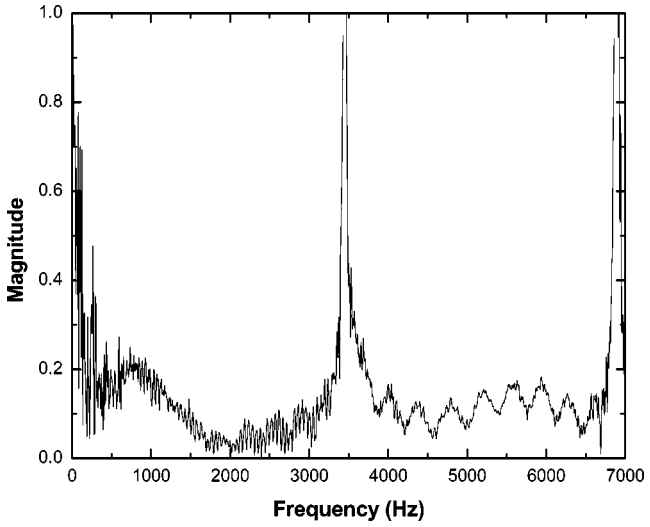

FIG. 3. Magnitude of the reflection factor of the downstream system.

magnitude lies below 0.3 at most frequencies. The peaks around 3500 Hz and 6900 Hz are believed to be due to the fact that the microphone spacing is a multiple of half-wavelengths and the calculation of reflection factor is indeterminate. More resonances may exist at frequencies beyond the cut-on frequency of the acoustic high modes (approximate 7000 Hz). The flow supply was designed for the use of different gas mixtures in the experiments. Use of different working fluids allows the variation of fluid properties, such as the viscosity and the sound speed. Three different helium–CO_2 mixtures, with helium mole ratios of 0, 0.33, and 0.57, were used in addition to air, allowing the speed of sound to be varied between 268 m/s and 409 m/s, and the viscosity to be varied between 8.4×10^{-6} m/s and 72.69×10^{-6} m/s^2.

Two flush-mounted microphones (6.35 mm diameter, B&K 4938) were installed along the tubes, each 14 cm upstream and downstream from the orifice plate, for the measurements of the radiated sound pressure. The background noise of the system, measured with the flow supply turned off was found to be negligible. Preliminary measurements were made using two microphones, with the second one installed 9 cm from the orifice plate. Measurement of the pressure frequency transfer function between the two microphones showed that the pressure disturbances propagated at the speed of sound. At very low frequencies, the microphone may have been in the acoustic near field and recorded pseudosound due to the turbulent structures which may not have been dissipated completely. This is believed to have induced some errors at low frequency in the identified M function and G_1 functions.

The output signals from the microphones were acquired at a sampling rate of 32 768 Hz using an HP356XA data acquisition system. The volumetric flow rate through the orifice was measured using a precision mass-flow meter (Baratron type 558A) at the inlet of the test section. The time-averaged pressure gradient across the orifice was measured using a pressure transducer (Baratron type 220C), with pressure taps installed along the tube as close as possible to the orifice plate.

IV. BROADBAND SOUND GENERATION

A. Straight orifice

Figure 4 shows radiated sound pressure spectra in air for different values of orifice pressure drop, Δp. The spectral level increases with the pressure drop, or the centerline velocity calculated using Bernoulli's equation

$$U=\sqrt{2\Delta p/\rho_0}, \tag{4}$$

where $\rho_0=1.2$ m^3/s is the medium density. Note that pressure heads in voice production studies are customarily reported in units of cm water.

The spectral decomposition method discussed in Sec. II was used to separate the acoustic frequency response function, the radiation efficiency function, and the source spectral distribution function. Figure 5 shows the resulting G_1 function. Additional curves showing He^2 and He^4 power laws are also shown in the figure for comparison. Following the discussion in Sec. II, the M function approximately obeys He^2 and He^4 trends at low and high He numbers, respectively, indicating a dominant quadrupole-type sound source. The corresponding source function, F, is shown versus the Reynolds number for constant Strouhal number, and versus the Strouhal number for constant Reynolds number in Figs. 6 and 7, respectively. Recall the hydraulic diameter is used as the characteristic dimension in the Reynolds number. The effects of Reynolds number were nearly negligible over the range from 200 to 20 000. This was expected since large scale turbulence contains most of the flow energy, and is sound radiation efficient. Increasing the Reynolds number implies finer grain turbulence in the flow, produced through the well-known cascading process. Small grain turbulence is spatially incoherent and thus contributes little to sound generation. Regressions show that the source function decreased approximately with the third power of the Strouhal number

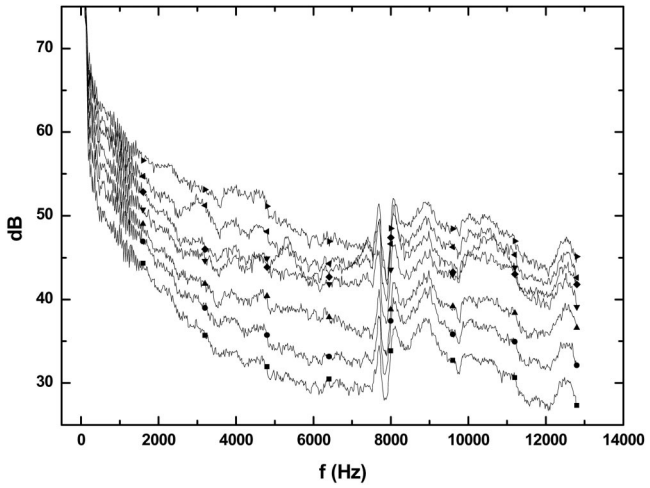

FIG. 4. Sound spectra measured for different transglottal pressure using air. Straight glottis-shaped orifice. ■, $\Delta p=8$ cm H_2O; ●, $\Delta p=10$ cm H_2O; ▲, $\Delta p=12$ cm H_2O; ▼, $\Delta p=14$ cm H_2O; ◆, $\Delta p=16$ cm H_2O; ◀, $\Delta p=18$ cm H_2O; ▶, $\Delta p=20$ cm H_2O.

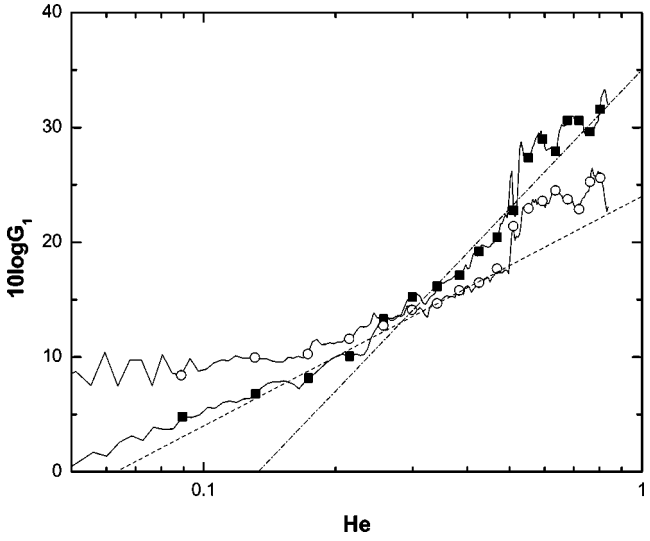

FIG. 5. Acoustic frequency response versus Helmholtz number. ■, straight glottis-shaped orifice; ○, convergent glottis-shaped orifice; - - -, 20 log He; -·-·-, 40 log He.

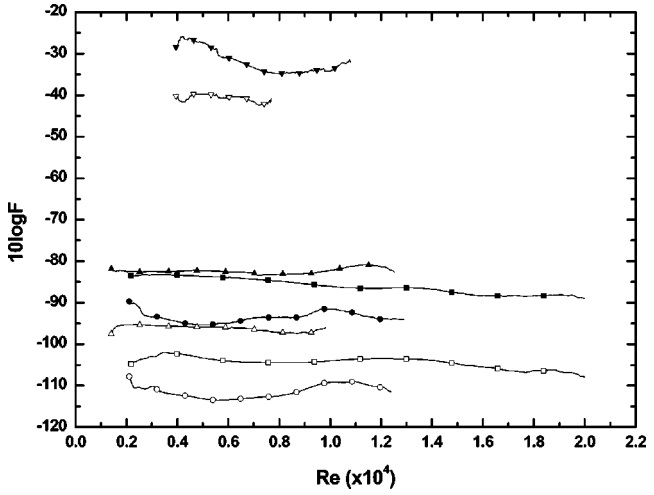

FIG. 6. Source spectral distribution function vs the Reynolds number at constant Strouhal numbers for different orifices. ■, circular orifice; ●, straight glottis-shaped orifice; ▲, convergent glottis-shaped orifice; ▼, free jets from divergent glottis-shaped orifice. Solid symbols, St=2; open symbols, St=5.

for Strouhal numbers smaller than one, and with the fifth power for Strouhal numbers greater than two, which is similar to the circular orifice case (Zhang *et al.*, 2002a).

B. Convergent orifice

Similar experiments were performed using a convergent glottis-shaped orifice. Figure 8 shows the sound spectra measured for air and different pressures. As in the case of straight orifices, the spectral amplitudes increase with jet velocity. The spectral decomposition method was applied and the resulting G_1 function is shown in Fig. 5. The G_1 function follows a He^2 trend at low Helmholtz numbers (up to around 0.45, the cut-on Helmholtz number for higher order acoustic modes), indicating a quadrupole-like sound source dominant at low frequencies. This is not surprising, as the flow within

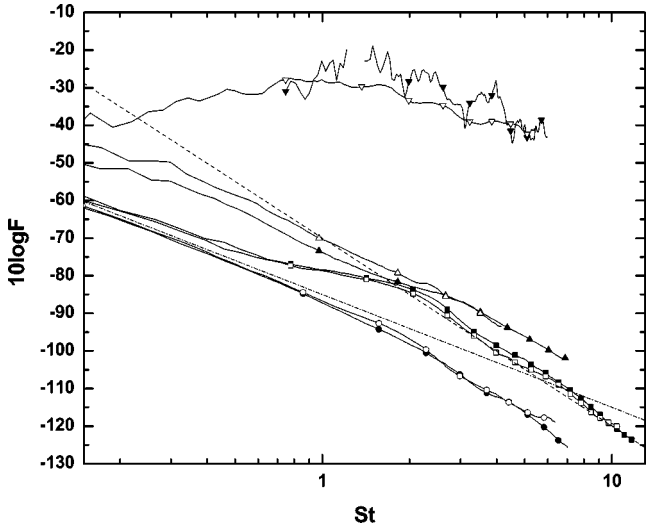

FIG. 7. Source spectral distribution function vs the Strouhal number at constant Reynolds numbers for different orifices. ■, circular orifice; ●, straight glottis-shaped orifice; ▲, convergent glottis-shaped orifice; ▼, free jets from divergent glottis-shaped orifice. Solid symbols, Re=4000; open symbols, Re=7000; - - -, −50 log St; -·-·-, −30 log St.

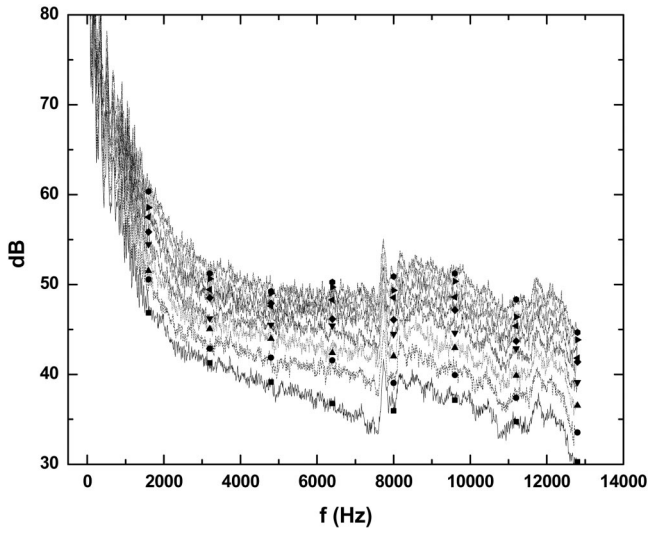

FIG. 8. Sound spectra measured for different transglottal pressure using air. Convergent glottis-shaped orifice. ■, $\Delta p = 10$ cm H_2O; ●, $\Delta p = 12$ cm H_2O; ▲, $\Delta p = 14$ cm H_2O; ▼, $\Delta p = 16$ cm H_2O; ♦, $\Delta p = 18$ cm H_2O; ◀, $\Delta p = 20$ cm H_2O; ▶, $\Delta p = 22$ cm H_2O; ⬢, $\Delta p = 24$ cm H_2O.

and immediately downstream the orifice is very stable (or ''laminar''), and turbulence appears further downstream into the tube (see discussion of Fig. 17 below). For greater Helmholtz numbers, the G_1 function deviates from a He^2 trend. The radiation function approaches at high frequency a He^4 law characteristic of a free field. Accurate regression at high Helmholtz numbers is difficult due to the presence of many resonances and sparse data points. At very low Helmholtz numbers the G_1 function is independent of Helmholtz number, which is partially due to flow supply noise. Another source of errors is the possible pseudosound recorded by the microphone, as discussed earlier in Sec. III.

The F function is plotted versus the Reynolds number and the Strouhal number in Figs. 6 and 7, respectively. Again, the effects of the Reynolds number were negligible. The spectral shape of the F function was very similar to that for the case of a straight orifice, following a St^{-3} trend at low Strouhal numbers, and St^{-5} at high Strouhal numbers.

C. Divergent orifice

The sound radiation characteristics of divergent orifices were different from those of the straight and convergent orifices. Figure 9 shows the sound spectra measured with air for mean pressure drops from 9 cm H_2O to 30 cm H_2O. Broadband levels seem to jump up for pressures above 10 cm H_2O. As the mean pressure drop further increases, level changes are frequency dependent. The sound levels are nearly constant within specific frequency bands, for example around 4 kHz. Near the Nyquist frequency of 12.8 kHz, the spectral level culminated for intermediate pressures around 18 cm H_2O.

Figure 10 shows similar sound spectra measured with CO_2 as the working fluid for norminal pressure drops from 10 cm H_2O to 26 cm H_2O. The nominal pressure drop is defined based on the density of air instead of the density of

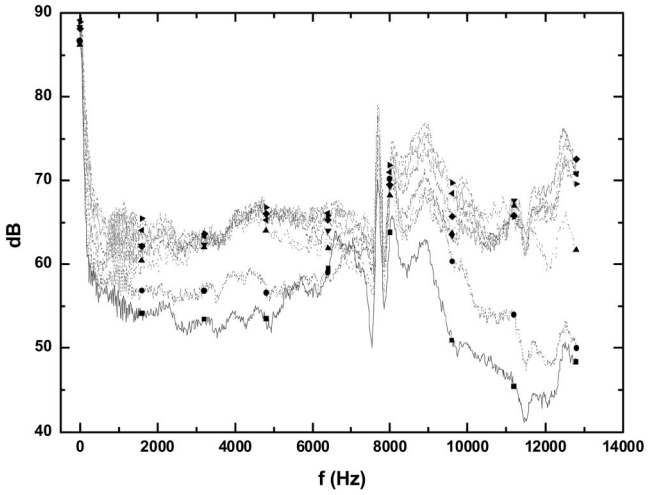

FIG. 9. Sound spectra measured at high flow rate in air. Divergent glottis-shaped orifice. ■, $\Delta p = 9$ cm H_2O; ●, $\Delta p = 10$ cm H_2O; ▲, $\Delta p = 14$ cm H_2O; ▼, $\Delta p = 18$ cm H_2O; ♦, $\Delta p = 22$ cm H_2O; ◀, $\Delta p = 26$ cm H_2O; ▶, $\Delta p = 30$ cm H_2O.

the specific gas mixture. Thus values of nominal transglottal pressure correspond to a given jet velocity, regardless of gas mixture. Since the sound speed is smaller in CO_2, the spectra extend to a larger He number. Two resonance frequencies (around 6000 Hz and 12 000 Hz) may be detected from the spectra. Again, the sound level at high frequencies culminated around 18 cm H_2O. The behavior above 8 kHz indicates that there may exist a tonal component of comparable amplitude at high flow rates at a frequency in between the two tube resonance frequencies. The tonal frequency increases with the jet velocity, and, when superimposed on the broadband component, may contribute to the complexity in the overall spectral shape and amplitude. This is discussed further in Sec. V.

Efforts were made to separate the source function using the spectral decomposition method. The resulting G_1 function, shown in Fig. 11, does not seem to obey a multipole power law of the type He^n as for the straight and diverging cases. Significant scattering from the ensemble mean

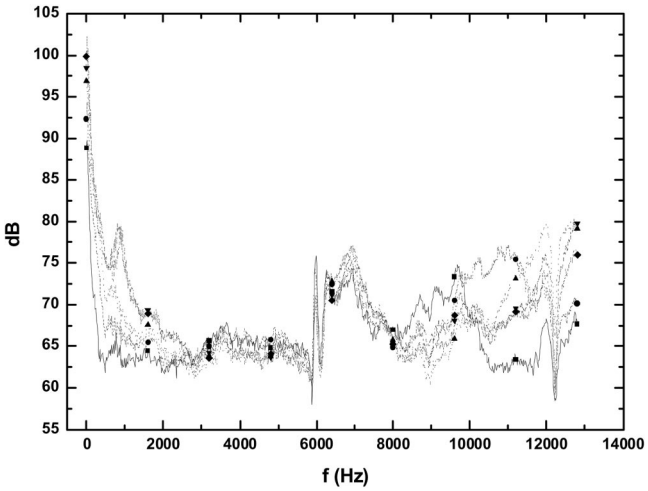

FIG. 10. Sound spectra measured at high flow rate in CO_2. Divergent glottis-shaped orifice. ■, $\Delta p = 10$ cm H_2O; ●, $\Delta p = 14$ cm H_2O; ▲, $\Delta p = 18$ cm H_2O; ▼, $\Delta p = 22$ cm H_2O; ♦, $\Delta p = 26$ cm H_2O.

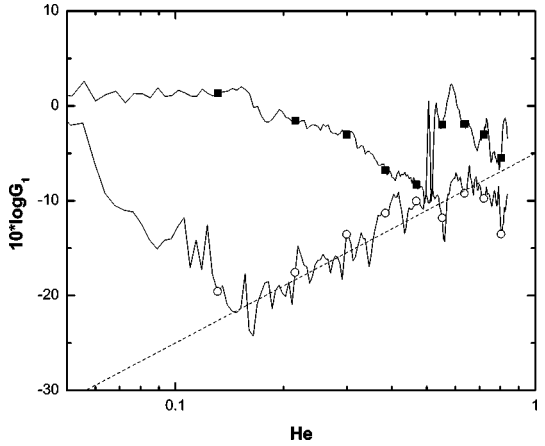

FIG. 11. Acoustic frequency response versus Helmholtz number. ■: divergent glottis-shaped orifice, confined flows; ○, divergent glottis-shaped orifice, free jet flows; - - -, 20 log He.

$10 \log F$ function was observed among the individual $10 \log F^k$ functions, with a standard deviation of 5 dB as compared to the approximate 15 dB dynamic range for $10 \log F$. Since it is unlikely any other sound generating mechanisms was present, this characteristic behavior was attributed to some kind of flow-acoustic interaction in this case. Vortex shedding, pairing, roll-up, and growth of instability waves are very sensitive to small acoustic disturbances. Any small disturbances reflected back to the orifice region could affect the near field flow, in particular flow separation and vortex shedding. A feedback loop may therefore exist. The confined tube configuration could definitely increase acoustic disturbances and enhance this kind of interaction, invalidating the basic source-filter model assumption.

This is substantiated by results obtained with the downstream tube removed, in an open jet configuration, shown in Fig. 12. The measurements were made on the jet axis, 16 cm away from the jet exit plane. The spectra are more predictable, with seemingly constant level increases with pressure,

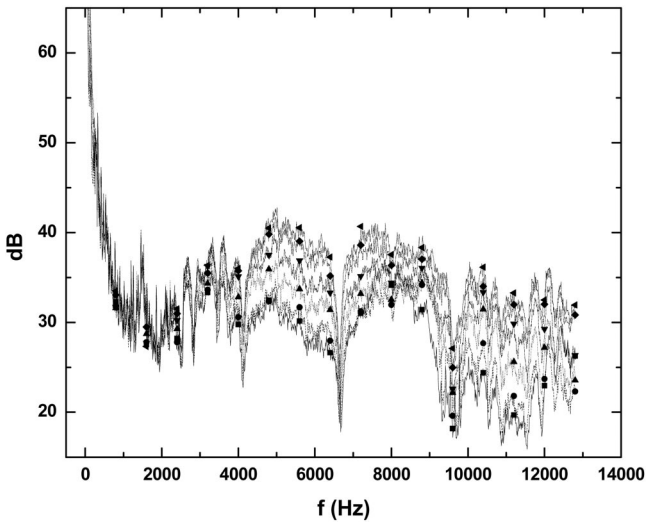

FIG. 12. Sound spectra measured at different high flow rate in air. Free jet flow through a divergent glottis-shaped orifice. ■, $\Delta p = 10$ cm H_2O; ●, $\Delta p = 12$ cm H_2O; ▲, $\Delta p = 16$ cm H_2O; ▼, $\Delta p = 20$ cm H_2O; ♦, $\Delta p = 26$ cm H_2O; ◀, $\Delta p = 30$ cm H_2O.

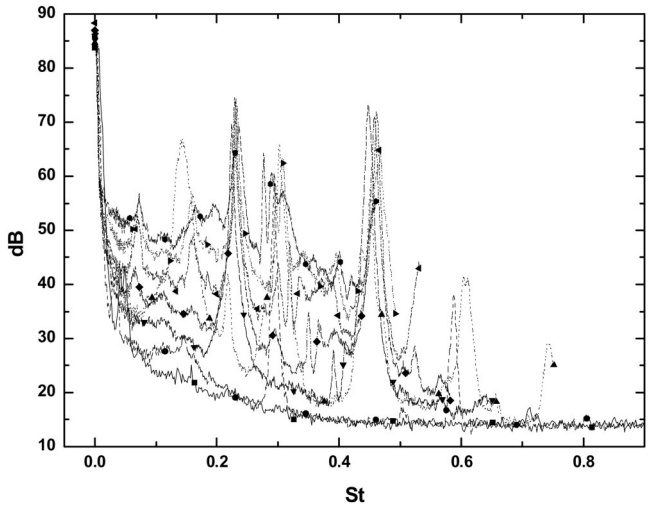

FIG. 13. Sound spectra measured at low transglottal pressures in air. Divergent glottis-shaped orifice. Pure tones were observed. ■, $\Delta p = 1$ cm H_2O; ●, $\Delta p = 2$ cm H_2O; ▲, $\Delta p = 3$ cm H_2O; ▼, $\Delta p = 4$ cm H_2O; ♦, $\Delta p = 5$ cm H_2O; ◀, $\Delta p = 6$ cm H_2O; ▶, $\Delta p = 7$ cm H_2O; ⬢, $\Delta p = 8$ cm H_2O.

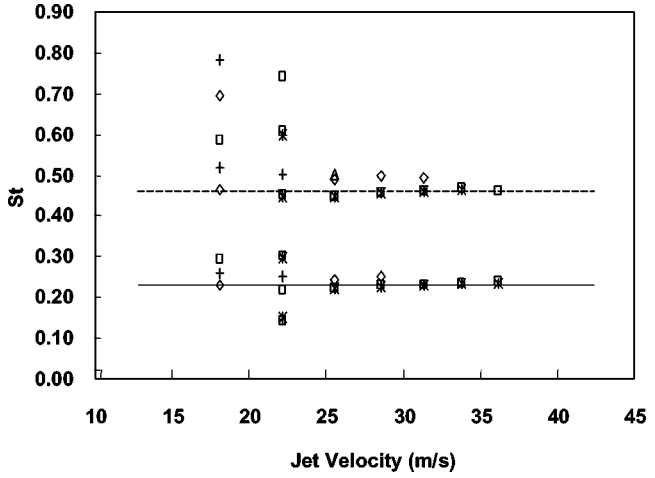

FIG. 14. The Strouhal number of the observed jet tones for a divergent glottis-shaped orifice versus the jet velocity. □, confined air jet; △, confined CO_2 jet; ◇, confined He–CO_2 jet;*, free air jet; +, free CO_2 jet;—, St = 0.23; - - -, St = 0.46.

except at low frequencies because of background noise attributed to the flow supply. The spectral decomposition method was again applied for this case. As shown in Fig. 11, the G_1 function follows a He^2 power law for mid- and high-Helmholtz numbers. This suggests that the sound source is dipolelike in this case (i.e., for a divergent orifice). Due to the unstable flow separation within the glottis, there exists significant interaction between the shed vortices and the orifice wall. The resulting dipole source then tends to dominate the sound field. The quadrupole source, which is associated with the turbulence region downstream of the orifice, is therefore less important. At lower Helmholtz number, the G_1 function tends to decrease with the Helmholtz number, which may again be due to significant background noise in the free jet configuration. Other errors may occur since the sound pressure measurements were made in the acoustic near field at low frequencies. The fluctuations in the G_1 function are believed to be due to reflections off surfaces near and downstream of the jet exit. The F function is plotted against the Reynolds number and the Strouhal number in Figs. 6 and 7, respectively. The source spectra culminate at midfrequencies. For Strouhal number values lower and higher than the peak Strouhal number, the F function approximately follows St^2 and St^{-2} trends, respectively.

The significant difference observed in the sound generation between the confined jet and free jet configurations for large flow velocities indicates that significant source-tube acoustic interaction may exist in the confined jet configuration for the divergent orifice shape. Such interaction was not evident in the results for the other orifice geometries studied.

V. TONAL SOUND GENERATION

Tonal sounds were produced for low flow rates through the stationary divergent orifice configurations, for flow velocities ranging from 17 to 37 m/s. Figure 13 shows typical sound pressure spectra measured with air for transglottal pressures between 1 cm H_2O and 8 cm H_2O. The frequency of the tones increased nearly linearly with the jet centerline velocity. As the jet velocity was increased, broadband sound increased gradually in level until it reached that of the tonal component. Eventually, as the transglottal pressure was increased above $\Delta p = 9$ cm H_2O (Fig. 9), the broadband component dominated although tones were still present in the spectra in some cases.

Figure 14 shows the Strouhal number of the tonal sounds versus the jet velocity. The hydraulic diameter of the orifice was used as the characteristic dimension in the definition of the Strouhal number. Both the fundamental, St ≈ 0.23, and the first harmonic, St ≈ 0.46, of the tonal sounds are shown. These values correspond to values reported for vortex shedding in shear layers, for example, for flow past a cylinder (Blake, 1986). It was found, by varying the working fluid, that the effects of viscosity on the tonal sounds Strouhal number were insignificant. The effects of the orifice dimensions are unknown, since the experiments were performed with the orifice area kept constant. At low flow rates (2 and 3 cm H_2O in air, or 18.08 and 22.14 m/s for the jet velocity), the fundamental Strouhal number was only 0.15 in one case, and Strouhal number values for tonal components were scattered over a range.

The tone Strouhal numbers and their onset velocities were consistent for different tube configurations. For example, radiated sound spectra measurements were repeated with the downstream tube removed to eliminate possible flow-acoustic loading feedback. The Strouhal numbers of the tonal sounds, shown in Fig. 14, were found to coincide with their confined jets counterparts. This suggests that the jet tones may be caused by a hydrodynamic phenomenon, and not by flow-acoustic interactions as the case of broadband sound generation at high flow rates discussed in Sec. IV C.

For one case, the instantaneous spanwise velocity profile within the jet was measured using a gated hot-wire probe located 0.5 mm downstream from the orifice exit. The probe was traversed every 0.1 mm along a 3 mm span, which in-

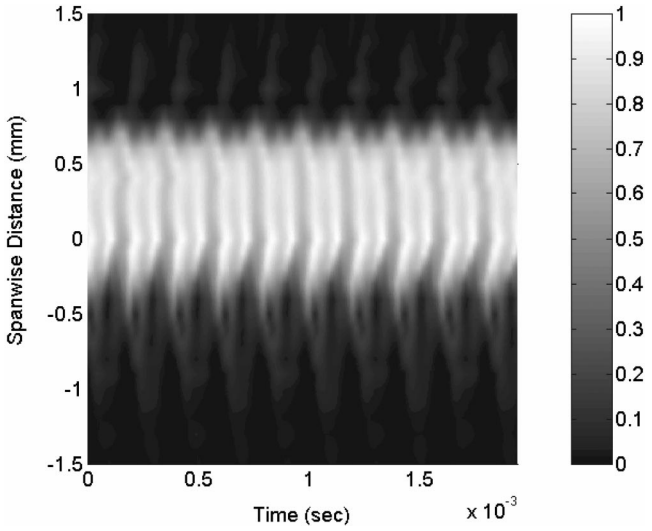

FIG. 15. Time history of the normalized jet velocity along the spanwise direction in presence of the jet tone. The center of the orifice is at the zero spanwise distance.

cluded the entire jet plume. The data acquisition was triggered and phase-locked at each location by using a filtered, nearly sinusoidal sound pressure signal from the microphone located in the tube upstream of the orifice. The instantaneous velocity profile for a few cycles is shown in Fig. 15. The frequency of the tone was 5.1 kHz, and the transglottal pressure 6 cm H_2O. The velocity oscillated in phase throughout the span of the orifice. The harmonic component at twice the fundamental frequency was strong. There was no apparent fluctuation in the jet core location over one cycle, and thus no apparent flipping of the jet plume from one diffuser wall to the other. The jet was permanently attached to one wall, as shown in Fig. 16, as found using an oil-based smoke injected into the air stream, and a strobe light. For a transglottal pressure of 10 cm H_2O, the jet plume is clearly skewed as a result of attachment to one of the glottal walls. It is not clear whether this was due to asymmetry in the orifice, or to a so-called Coanda effect. The jet plume discharge angle was bi-stable, and could be manipulated through slight adjustments in the orifice geometry. With very careful positioning, the jet plume was normal to the exit plane in a state of unstable equilibrium.

It is possible that shear layer instabilities within the jet may cause a slight shift in the flow separation point within

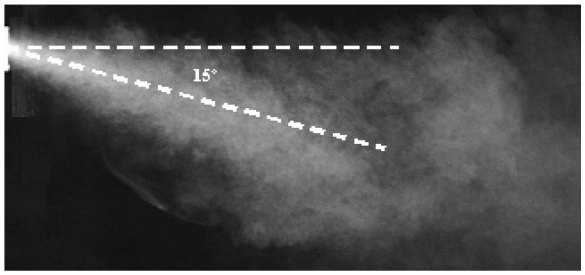

FIG. 16. Flow visualization of steady free jet just beyond divergent orifice. The orifice exit plane roughly corresponds to the left edge of the image. It can be seen that the jet is here attached to the lower surface of the orifice, causing it to exit at an angle corresponding to orifice wall angle (15°).

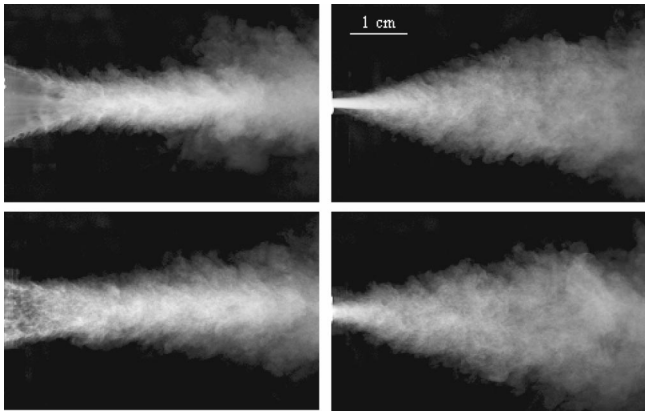

FIG. 17. Flow visualization of free jet just beyond the convergent (top) and divergent (bottom) orifices. $\Delta p = 4$ cm H_2O. The jet in the first 5 to 10 mm is clearly more stable in the convergent case than for the divergent case.

the divergent orifice. This could change the flow resistance of the orifice and result in a surge, or periodic ''blocking'' of the orifice. Note that this phenomenon did not occur for convergent orifices. Flow separation, or stall, is known to occur under adverse pressure gradient for jet flows through divergent channels. Over a certain range of diffuser angle and ratio of orifice length to orifice throat width, large transitory stalls occurs and the entire flow region is characterized by a large, low frequency surge or stall (Kline, 1959). Such dynamic stall induces pressure fluctuations and unsteady flow behavior both upstream and downstream of the orifice (Smith, 1975). Similar observations were made in studies of jets flow through knife-edge orifices by Johansen (1929), and Beavers and Wilson (1970). Vortical structures shed at a constant Strouhal number over the range $200 < \mathrm{Re} < 3500$ were observed. The Strouhal number observed of the vortical structures for the two-dimensional orifice was around 0.43, which is approximately twice the value for the jet tone observed in present study. This could be accounted for by vortex pairing, with subharmonics excited and contributing to the sound radiation. At low flow rates, paired vortices may pair again with another vortex giving rise to oscillations at one-third of the vortex shedding frequency in the sound field.

VI. EFFECTS OF ORIFICE GEOMETRY

For the cases of a circular straight orifice (Zhang *et al.*, 2002a), as well as for the straight and convergent glottis-shaped orifices, the flow within and immediately downstream of the orifice is laminar and stable. Instability waves appear several orifice diameters downstream, beyond which the flow transitions to turbulence abruptly. Figure 17 shows two pictures of the flow just downstream of the orifice exit plane for the convergent orifice (unconfined flow). The laminar core may be seen, along with vortical structures generated downstream due to shearing and mixing. The sound generation process for these cases exhibits all more of a quadrupole type behavior, which may due to the fact that turbulence appears several glottal diameters downstream in the tubes and thus there is less random force fluctuations on the orifice. The source functions for these three cases follow

similar spectral similarity laws. Note for convergent shapes, Fig. 17, the merging or collision of the corner vortices could affect the quadrupole source strength.

For a divergent orifice, the flow is turbulent right beyond the glottis exit as shown in Fig. 17 for one free divergent jet and 4 cm H_2O transglottal pressure. The flow separates within the orifice and is very sensitive to small disturbances. The resulting hydrodynamic and acoustic feedback loops are responsible for the tonal sound observed at low flow rates and the turbulent sound spectral behavior at high flow rates, respectively.

Although the divergent orifice geometry has significant effects on the flow field and sound generation process in the steady jet flows, it is not clear that whether these observed feedback mechanisms would occur in the unsteady flow configuration, as in voice production. It is possible these feedback loops may not have enough time to develop considering the constantly changing pulsating flows. On the other hand, the source spectral distribution functions for the other two orifice geometries and the circular orifices have been shown to follow similar trends. This scaling law in the source spectral shape and amplitudes may be used for the noise modeling in high-quality speech synthesis.

VII. CONCLUSIONS

Experiments were performed to study sound radiation from stationary jet flows through glottis-shaped orifices. Three orifice geometries were studied with straight, divergent, and convergent profiles. For the straight and convergent orifices, the sound generation characteristics were found to be similar to those of circular orifices, i.e., quadrupole type of source. The source spectral distribution functions for the two orifice geometries follow similar trends, decreasing approximately with the third power and fifth power of the Strouhal number at low and high Strouhal numbers, respectively. For the divergent orifice, jet tones were produced at low flow rate, with a fundamental Strouhal number around 0.23, which is probably related to a dynamic surge phenomenon. At high flow rates, the sound field is dominated by broadband sound. Significant differences in the sound field between the confined divergent jets and the free divergent jets were observed at high flow rates. The free jet sound was found to be a dipole type of source. The confined jets exhibit a different complex behavior, which is probably due to flow-acoustic interactions and the existence of a feedback loop. Extended flow visualization and detailed flow measurements are needed to further understand the flow field and characterize possible sound generation mechanisms.

ACKNOWLEDGMENTS

This study was supported by Research Grant No. RO1 DC03577-06 from the National Institute of Deafness and Other Communication Disorders, National Institutes of Health.

Barney, A., Shadle, C. H., and Davies, P. O. A. L. (**1999**). ''Fluid flow in a dynamic mechanical model of the vocal folds and tract. I. Measurements and theory,'' J. Acoust. Soc. Am. **105**, 444–455.

Beavers, G. S., and Wilson, T. A. (**1970**). ''Vortex growth in jets,'' J. Fluid Mech. **44**, 97–112.

Blake, W. K. (**1986**). *Mechanics of Flow-Induced Sound and Vibration* (Academic, New York).

Dabiri, J., Kucinschi, B., Afjeh, A., Dewitt, K., Scherer, R., and Agarwal, M. (**2001**). ''Smoke flow visualization for the flow through a symmetrical and an oblique glottis with and without the presence of the false vocal folds,'' Research report, Optical flow diagnostics laboratory, University of Toledo.

Davies, H. G., and Ffowcs Williams, J. E. (**1968**). ''Aerodynamic sound generation in pipe,'' J. Fluid Mech. **32**, 765–778.

Flanagan, J. L. (**1965**). *Speech Analysis, Synthesis, and Perception* (Springer-Verlag, Berlin).

Goldstein, M. E. (**1976**). *Aeroacoustics* (McGraw-Hill, New York).

Harper, V. H. (**2000**). ''Respiratory tract acoustical modeling and measurements,'' Ph.D. thesis, Purdue University, West Lafayette.

Hofmans, G. C. J. (**1998**). ''Vortex sound in confined flows,'' Ph.D. thesis, Universiteis-drukkerij, TUE, Ben Mobach, TUE.

Howe, M. S. (**1998**). *Acoustics of Fluid-Structure Interactions* (Cambridge University Press, Cambridge).

Johansen, F. C. (**1929**). ''Flow through pipe orifices at low Reynolds numbers,'' Proc. R. Soc. London, Ser. A **216**, 231–245.

Kline, S. J. (**1959**). ''On the nature of stall,'' J. Basic Eng. **81**, 305–320.

McGowan, R. S. (**1988**). ''An aeroacoustic approach to phonation,'' J. Acoust. Soc. Am. **83**, 696–704.

Meyer-Eppler, W. (**1953**). ''Zum Erzeugunsmechanismus der Geraus-chlaute,'' Zeitschrift fur Phonetik und allgemeine Sprachwissenschaft, **7**, 196–212.

Moore, C. J. (**1977**). ''The role of shear-layer instability waves in jet exhaust noise,'' J. Fluid Mech. **80**, 321–367.

Shadle, C. H., Elliott, S. J., and Nelson, P. A. (**1987**). ''Visualization of the air flowing through a dynamic model of the vocal folds,'' ISVR Technical Report 154.

Smith, C. R. (**1975**). ''A note on diffuser generated flow unsteadiness,'' J. Fluids Eng. **97**, 377–379.

Stevens, K. N. (**1998**). *Acoustic Phonetics* (The MIT Press, Cambridge, MA).

Zhang, Z., Mongeau, L., and Frankel, S. H. (**2002a**). ''Broadband sound generation by confined turbulent jets,'' J. Acoust. Soc. Am. **112**, 677–689.

Zhang, Z., Mongeau, L., and Frankel, S. H. (**2002b**). ''Experimental verification of the quasisteady approximation for aerodynamic sound generation by pulsating jets in tubes,'' J. Acoust. Soc. Am. **112**, 1652–1663.